Biosensors and Bioelectronics 127 (2019) 10–18

Contents lists available at ScienceDirect

Biosensors and Bioelectronics

journal homepage: www.elsevier.com/locate/bios

Functionalized nitrogen doped graphene quantum dots and bimetallic Au/Ag core-shell decorated imprinted polymer for electrochemical sensing of anticancerous hydroxyurea

Purnendu Kumar Pathak[1], Anil Kumar[1], Bhim Bali Prasad*

Analytical Division, Department of Chemistry, Institute of Science, Banaras Hindu University, Varanasi 221005, India

ARTICLE INFO

Keywords:
Nitrogen doped graphene quantum dots
Iniferter
Molecularly imprinted polymer
Bimetallic Au/Ag core shell
Hydroxyurea

ABSTRACT

A novel molecularly imprinted polymer-capped acrylated nitrogen doped graphene quantum dots and bimetallic Au/Ag core-shell was synthesized to serve as a sensing nano-hybrid film for the detection of an anticancerous drug, hydroxyurea. This exploited the use of a functionalized nitrogen doped graphene quantum dots iniferter. This initiated the polymerization, following "surface grafting-from" approach, over the surface of a screen-printed carbon electrode to obtain requisite stability and selectivity of the measurement. Herein, nitrogen doped graphene quantum dots were prepared utilizing the degree of dehydration/carbonization of citric acid (carbon skeleton) and urea (nitrogen dopant) as source materials. This provided an efficient sensor platform anchoring bimetallic Au/Ag core-shell on its surface. The nano-assembly of acrylated nitrogen doped graphene quantum dots and bimetallic Au/Ag core-shell@imprinted polymer actually amplified the electrode kinetics by improving the diffusion coefficient (~20-fold) and electron-transfer kinetics (~5-fold), in comparison to the simple bimetallic Au/Ag core-shell decorated imprinted sensor. Under optimized conditions of differential pulse anodic stripping voltammetric transduction, a linear relationship between the current and the concentration was obtained in the range of 0.62–102.33 ng mL^{-1} for hydroxyurea. The detection limit was observed to be 0.07 ng mL^{-1} in blood plasma, without having any matrix effect, cross-reactivity, and false-positives. The proposed sensor assures its clinical applicability for the treatment of cancer.

1. Introduction

Molecularly imprinted polymers (MIPs) are tailor-made synthetic receptors with high recognition binding affinity for target molecules. However, the homogeneous cavities in MIP motif could be generated with the use of an iniferter, nitrogen doped graphene quantum dots (N-GQDs), for the covalent linkages with MIP functionality. Moreover, metal nanoparticles such as gold nanorods (Au NRs) can provide proficient support for the electrochemical sensing of drugs and biomolecules, on account of high surface area, efficient mass transport, and good biocompatibility (Sun et al., 2015). Especially, bimetallic nanoparticles enhance magnetic, optical and catalytic properties in comparison with the monometallic nanoparticles. This is presumably due to unique inter-particle interactions in bimetallic composition causing excellent synergism in the two metals for promoting molecular adsorption and activation (Dai et al., 2017; Hsu et al., 2011). In this context, the core-shell nanostructure of Au/Ag bimetallic (Au/Ag NRs) have attracted much attention in the field of sensing (Ma et al., 2010; Maier and Atwater, 2005; Samal et al., 2013; Jiang et al., 2011; Endo et al., 2006).

The metal based nanomaterials were found to reveal electro-catalysis, avoiding their aggregation with the support of suitable carbon based nanomaterials (Wang et al., 2017). Of several carbon polymorphs, two-dimensional graphene-based materials have been used to enhance the electro-catalysis on account of their excellent conductivity, large specific surface area, and high charged carrier mobility (Chen et al., 2018a, 2018b; Geng et al., 2015; Wang and Su, 2014; Choi et al., 2012). However, the zero-band gap carbon based materials with sizes less than 10 nm, called graphene quantum dots (GQDs), are more advantageous. These materials can be obtained by tuning their electronic properties with the variation in size and edge structure of graphene from zero band-gap metallic to a finite band-gap semiconductor. Besides their small sizes, GQDs can trap electrons in their quantum confinement and enhance sensitivity by promoting electron transfer toward

* Corresponding author.
E-mail address: prof.bbpd@yahoo.com (B.B. Prasad).
[1] Equally contributed.

https://doi.org/10.1016/j.bios.2018.11.055
Received 25 September 2018; Received in revised form 19 November 2018; Accepted 30 November 2018
Available online 07 December 2018
0956-5663/

the electrode surface. Subsequently, the doping of nitrogen into GQDs, yielding N-GQDs, might tailor the electronic properties and separate the charges generated at the interface paving the pathway for charge transport to the electrode surface (Y.Li et al., 2012; Q.Li et al., 2012). Notably, N-GQDs are prepared either by the use of "top–down" or "bottom–up" approach. The "top–down" approach refers to figure bulk carbon materials into tiny GQDs, followed by nitrogen doping. But, this suffers from low yield and encounters difficulties in controlling the shape and size distribution (Dong et al., 2012). However, the "bottom-up" approach is more advantageous in terms of compositional tuning by controlling the size and shape of N-GQDs, with the help of suitable organic precursors. Various researcher utilized pristine GQDS and N-GQDs as sensing materials (Lin et al., 2015; Cai et al., 2014; Kashani et al., 2017; Shi et al., 2015; Tam et al., 2014; Ju and Chen, 2014; Li et al., 2015; Jiang et al., 2014; Wang et al., 2010; Kumawat et al., 2017; Aoun, 2017; Zhao et al., 2011; Roushani and Abdi, 2014; Razmi and Mohammad-Rezaei, 2013). A very few researchers exploited pristine GQDS and N-GQDs for MIPs fabrication (Yang et al., 2017; Amjadi and Jalili, 2016; Tan et al., 2016; Zhou et al., 2015; Zor et al., 2015). However, these modified sensors were found to suffer from acute problem of GQDs leaching either from the electrode surface or from the imprinted nanocomposite to the solution, during measurement of response signal. Thus, the best way could be the use of the stabilized (functionalized) form of GQDs for the sensor fabrication. The stabilized monomeric-GQD was reportedly synthesized by oxidative cutting of graphene oxide using "top-down" approach (Prasad et al., 2017), which required the multiple steps of complex manipulation. This enigma was resolved in present work by exploring the "bottom-up" approach. This was followed by the functionalization of N-GQDs as acrylated N-GQDs to achieve stability of the polymer motif *via* covalent linking with monomer. In "bottom up" approach the one-step hydrothermal (Qu et al., 2014) process was employed for the synthesis of N-GQDs using precursors citric acid (CA) as a carbon and urea as nitrogen source materials, in aqueous media. Hydrothermal process is generally preferred one, as it does not require expensive reagents and organic solvents including further surface passivation. Furthermore, N-GQDs have many anchoring sites for the adsorption of metal ions (Chizari et al., 2010), such as Au/Ag bimetallic nanoparticles in the present case. We have endeavored, for the first time, to exploit a nanohybrid comprised of acrylated N-GQDs and bimetallic (Au/Ag) nano-rods for MIP fabrication at iniferter N-GQDs modified screen printed carbon electrode (Au/AgNRs@N-GQDs-MIP/SPCE). This was found very useful for the selective and sensitive detection of hydroxyurea (HU).

The model target HU is an antineoplastic agent with cytotoxic activity, which blocks DNA synthesis by inhibiting the enzyme ribonucleotide reductase. This is used in the treatment of cancer, sickle cell anemia, and human immunodeficiency virus (HIV) infection. Its therapy causes some side effects such as neutropenia, bone marrow suppression, elevation of hepatic enzymes, anorexia, nausea, vomiting, and infertility. There were several chromatographic methods for HU determination such as isocratic reverse phase high performance liquid chromatography (RP-HPLC) (Gordon et al., 2015), gas chromatography–mass spectrometry (James et al., 2006; Kettani et al., 2009), ultra HPLC (Elias et al., 2014), HPLC method coupled with UV (Bachir et al., 2007), HPLC coupled with tandem mass spectrometry (Hai et al., 2017; Usawanuwat et al., 2014), HPLC coupled with electrospray ionization tandem mass spectrometry (Marahatta et al., 2016), liquid chromatography with electrochemical detection (Rodriguez et al., 2014; Jong et al., 2003), including spectrophotometric determination (Majid and Bashir, 2013). However, these methods lacked sensitivity and selectivity and required sophisticated instrumentations. Alternatively, the electrochemical detections of HU were attempted to achieve the fast response, easy to handle, good stability, portability, and the low cast (Naik et al., 2015, 2013; Naik and Nandibewoor, 2014). However, these sensors still lacked sensitivity and selectivity in the complex matrices. Moreover, several critical problems like high overpotential and sluggish electrode kinetics may be problematic. In order to overcome these attendant problems, MIPs could be considered viable for the sensitive and selective molecular recognition. In this context, only quantum chemical study evoking second order Moller Plesset (MP2) calculation is reported (Prasad and Rai, 2013). Thus, a genuine surge is required for the development of selective and sensitive MIP-based electrochemical sensor for HU analysis in real samples.

2. Experimental

2.1. Reagents

All solvents, used throughout the experiment, were obtained from Spectrochem Pvt. Ltd and Loba chemie (Mumbai, India). The chemicals CA, urea, maleic anhydride, p-toluene sulphonic acid, sodium bicarbonate, acryl amide, $SOCl_2$, dopamine (DA), SDD, and CS_2 were purchased from Loba chemie (Mumbai, India). $AgNO_3$ was purchased from E-Merck Ltd. (Mumbai, India). Test analyte HU, crosslinker (ethylene glycol dimethacrylate), and all interferences were obtained from Sigma-Aldrich (Steinheim, Germany), Fluka (Steinheim, Germany) and TCI (Tokyo, Japan). The pharmaceutical formulation analyzed was Cytodrox (HU, 500 mg per capsule) which was purchased from Cipla pharmaceutical Ltd. (India). The real samples (Human urine and blood plasma) used in this work, were procured from the pathology division of Institute of Medical Science Banaras Hindu University (Varanasi, India) and stored in a refrigerator at −4 °C, before use. To diminish the matrix effect to a larger extent during analysis, the dilution of the real samples was requisite. Any pretreatment (centrifugation, ultrafiltration, deprotenization, *etc.)* of these samples was avoided, since it might lead to inaccuracies in the final analytical results. The HU solution (500 μg mL^{-1}) was prepared in the demineralized tripled distilled water (conducting range: 0.06–0.07 $\times 10^{-6}$ S cm^{-1}) and a fresh solution was used throughout the experiment. As the supporting electrolyte, phosphate buffer (pH 7.5, 0.1 M) was used and as per requirement their pH values were adjusted with the addition of a small amount of either acid (0.1 M HCl) or base (0.1 M NaOH).

2.2. Apparatus

Cyclic voltammetry (CV) and differential pulse anodic stripping voltammetry (DPASV) measurements were performed, using a portable potentiostat μ-Stat 200 (Drop Sens S.L. Oviedo) connected to a personal computer and SPCE. Chronocoulometry were recorded with an electrochemical analyzer (CH instruments, USA, model 1200 A) using the same electrode assembly. UV–vis spectra were recorded on Varian Cary 100 Bio UV–visible spectrophotometer (USA). Fourier transform infrared (FT-IR) spectra were studied on Varian 3100 FT-IR (USA) spectrometer, using KBr thin pellet containing the sample. Raman scattering measurements were carried out on a Renishaw in Via-plus micro-Raman system, at the room temperature, with 532 nm excitation wavelength. Morphology of N-GQDs, AuNRs, and Au/Ag NRs were examined by transmission electron microscopy (TEM, Technai-12FEI Eindhoven, Netherlands), assembled with EDAX detecting unit (Technai-20(ST), 136–10, Port EDS, amplifier model 204) to record energy dispersive X-ray spectra (EDS). Surface morphologies of MIP-adduct and MIP were studied using high resolution scanning electron microscope (SEM, Nova Nano-sem 450 FEI, Netherlands) and atomic force microscope (AFM, NT-MDT, Russia). Brunauer-Emmett-Teller (BET) analysis of nanocomposites (Au/AgNRs-MIP and Au/AgNRs@N-GQDs-MIP) were performed using a micromeritics ASAP 2020 apparatus at the temperature of liquid nitrogen −195.56 °C for obtaining surface area of polymer motifs. Ultrathin coatings of iniferter and prepolymer solution over the SPCE surface were made using a standard spin-coater (ACE→ 200, Dong Ah Tech, Seoul, South Korea).

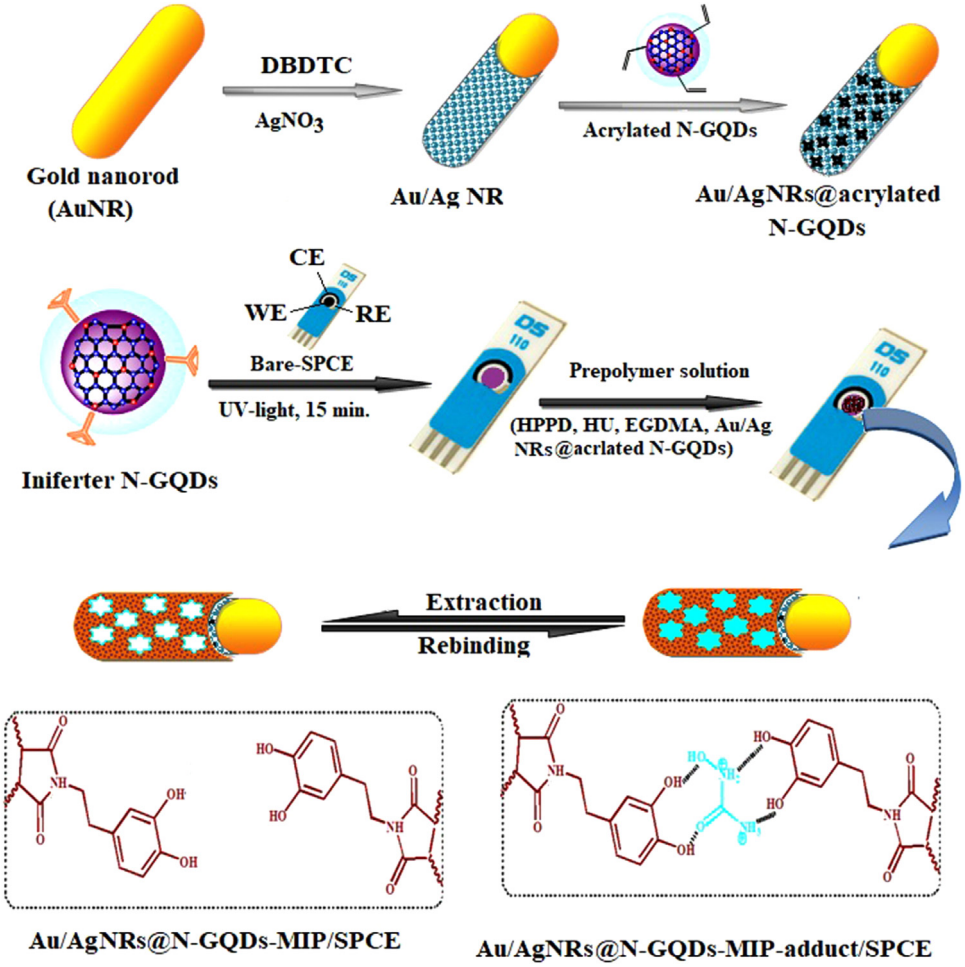

Scheme 1. Schematic illustrations of Au/AgNRs@acrylated N-GQDs synthesis and its subsequent fabrication as Au/AgNRs@N-GQDs-MIP modified SPCE.

2.3. Synthesis of functional monomer

The functional monomer, 1-(2-(3, 4- Dihydroxy-phenyl)-ethyl)-pyrrole-2,5-dione (HPPD), was prepared based on a known recipe (Gowda and Mahendra, 2006). In brief, DA and maleic anhydride (20 mmol each) were mixed in DMF with stirring for 2 h, followed with addition of p-toluene sulphonic acid (1 mmol). The resulting product was filtered, washed with 5% sodium bicarbonate solution, and characterized (FT-IR (KBr, cm^{-1}): 3353 (O-H), 1707 (-C=O), 1627 (C=C), and 1536 (C=C aromatic ring stretch)).

2.4. Preparations of N-GQDs, N-GQDs-COCl, iniferter N-GQDs, and acrylated N-GQDs

N-GQDs were synthesized following a "bottom up" method (Scheme S1) (Qu et al., 2014). Herein, CA (15 mmol) and urea (5 mmol) were first dissolved in water (25 mL). This was transferred into a Teflon lined stainless autoclave and heated to 160 °C for 6 h. After cooling to the room temperature, ethanol was added and the resulting product was collected through the centrifugation at 10,000 rpm for 30 min. N-GQDs were converted to N-GQDs-COCl by refluxing with $SOCl_2$ and subsequent washing with THF.

For the synthesis of iniferter N-GQDs, SDD (250.0 mg) was dissolved in ethanol under nitrogen atmosphere and N-GQDs-COCl suspension (25.0 mg, 2 mL ethanol) was added drop-wise into it in cold condition, with the intermittent stirring for 24 h. The final product was collected by centrifugation and dried under vacuum.

For the preparation of acrylated N-GQDs, N-GQDs-COCl (25.0 mg) and acryl amide (250.0 mg) were dispersed in 20 mL anhydrous THF and refluxed at 80 °C for 24 h. The final acrylated N-GQDs were collected by centrifugation, washed several times with ethanol, and finally dried at 100 °C for 24 h.

2.5. Synthesis of bimetallic Au/Ag NRs

Au/Ag NRs were prepared following a known procedure (Huang et al., 2013a, 2013b). For this, AuNRs were first prepared on the basis of a classical seed-growth method (Ye et al., 2013; Huang et al., 2013a, 2013b). In brief, a seed solution was made by adding a freshly prepared ice cold aqueous $NaBH_4$ solution into a mixture of $HAuCl_4$ and cetyl trimethylammonium bromide (CTAB) aqueous solution, with vigorous stirring (1200 rpm) and kept standstill at the room temperature. A growth solution was made by the addition of $AgNO_3$ solution into the mixtures of CTAB and sodium oleate in aqueous medium at 30 °C for 15 min. Subsequently, $HAuCl_4$ solution was added into it under magnetic stirring. After half-an-hour, HCl solution (2.1 mL, 12.1 M) was added followed by the addition of ascorbic acid solution (1.25 mL) into reaction vessel with stirring. Both growth and seed solutions were mixed with stirring (1500 rpm) for 30 s and finally kept, without any disturbance at 30 °C for 12 h. This gave rise to the production of AuNRs, which was collected by the centrifugation at 10,000 rpm. Afterward, AuNRs were dispersed in the CTAB solution (80 mM) and mixed with (3,4-dihydroxy-benzyl)-dithiocarbamate (DBDTC) solution. Herein, DBDTC was already prepared by the reaction of equimolar mixture of DA and CS_2 (Kailasa and Wu, 2012). For sufficient adsorption of DBDTC on AuNRs, the above reaction mixture was allowed for sonication

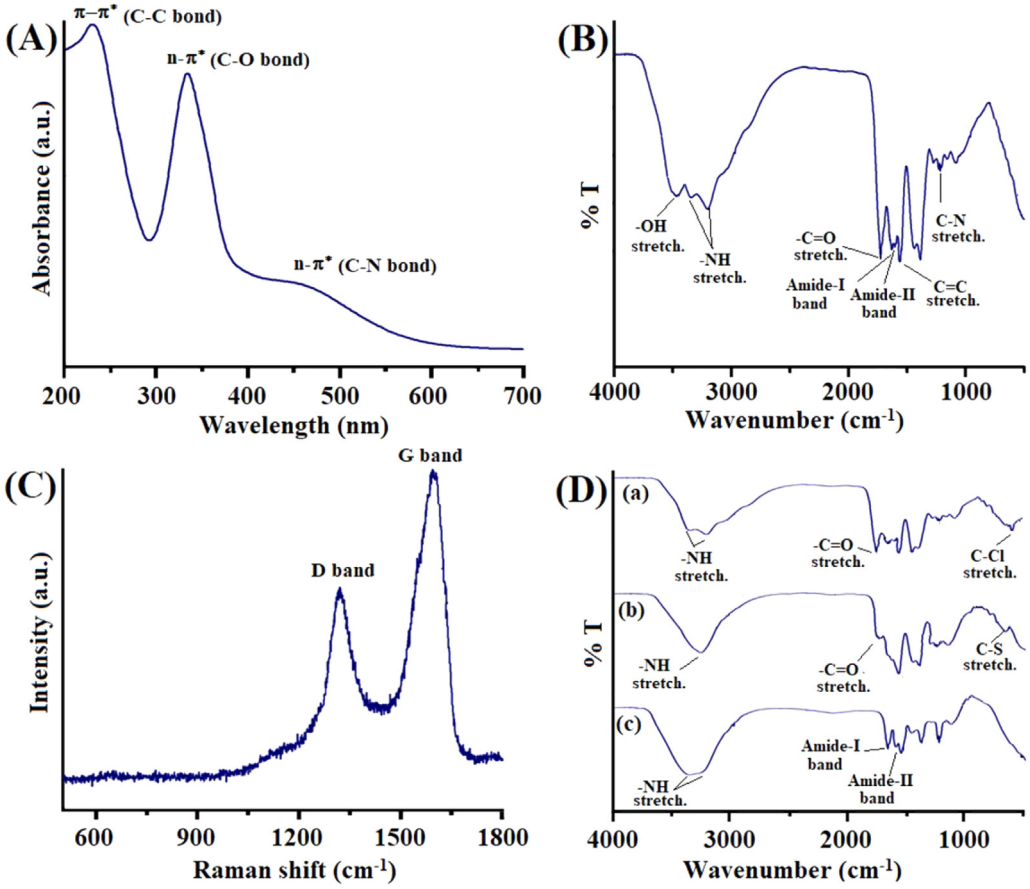

Fig. 1. (A) UV–vis spectrum of N-GQDs, (B) FT-IR (KBr) spectrum of N-GQDs, (C) Raman spectrum of N-GQDs, and (D) FT-IR (KBr) spectra: N-GQDs-COCl (curve a), iniferter N-GQDs (curve b), and acrylated N-GQDs (curve c).

(5 min) and stirred for 12 h. Subsequently, $AgNO_3$ (100 µL, 0.01 M) was added into reaction vessel and sonicated for the additional 5 min. Finally, the resultant solution was left undisturbed at 65 °C for 4 h for the growth of Ag shell on AuNRs.

2.6. Electrode fabrication

The SPCE used for this work was consisted of a working electrode (WE, carbon, 4 mm diameter), a counter electrode (CE, carbon) and a reference electrode (RE, silver). SPCE was chosen, as it is advantageous toward the electrochemical sensing, on account of its reproducibility and scalability (Das and Sangaranarayanan, 2015; Zhang et al., 2000; Liu et al., 2001). It rendered reproducible voltammograms when electrochemically swept between − 0.5 and + 1.0 V, in 0.5 M H_2SO_4 at 0.1 Vs^{-1} (Vasilescu et al., 2003). The counter (carbon) and reference (silver) electrodes of SPCE were safely covered with Teflon tape and working electrode was allowed for the modification. Later, Teflon tape was removed out during analytical measurements.

The SPCE was modified as discuss below (Scheme 1):

2.6.1. Immobilization of iniferter at SPCE

The aqueous suspension of iniferter N-GQDs (10 µL, 1 mg mL^{-1}) was placed on working electrode area of SPCE and spin-coated for 15 s. Herein, iniferter N-GQDs were adsorbed onto the micro porous graphitic SPCE surface by π-π interactions and physi-sorption. Afterward, iniferter N-GQDs modified SPCE was irradiated in UV chamber (delivering 9 Wcm^{-2}) for 15 min.

2.6.2. Immobilization of MIP on iniferter N-GQDs modified SPCE

The “surface-grafting from” approach was adapted to develop an exterior layer of MIP on the iniferter N-GQDs modified SPCE. Accordingly, the template (HU, 0.1 mmol/400 µL DMSO) and the monomer (HPPD, 0.2 mmol/600 µL DMSO) were mixed and allowed for the self assembly in half an hour. Subsequently, the suspension mixture of acrylated N-GQDs and Au/Ag NRs (200 µL, 2 mg mL^{-1}) was added, in inert condition, in the presence of a cross-linker (ethylene glycol dimethacrylate, 1 mmol). Finally, 10 µL of this pre-polymer mixture was placed on the iniferter N-GQDs modified SPCE and spin coated at 2600 rpm for 15 s. The modified SPCE was placed in UV chamber with intermittent irradiation for 4 h to initiate photo-graft surface polymerization. All template molecules were retrieved from the exterior MIP-adduct layer with methanol for 30 min, under dynamic condition. The complete removal of template molecule was ensured by obtaining no voltammetric current response. This gave rise to the fabrication of MIP modified SPCE (Au/AgNRs@N-GQDs-MIP/SPCE). A non-imprinted polymer (NIP) modified electrode (Au/AgNRs@N-GQDs-NIP/SPCE) was also prepared in the similar manner, but in the absence of the template. Au/Ag NRs-MIP modified SPCE was also prepared for the comparison studies.

Polymerization conditions (template-monomer stiochiometry (1:2), monomer-crosslinker (1:5), suspension of acrylated N-GQDS and Au/Ag NRs (200 µL, 4:1, w/w ratio), and polymerization time (4 h)) utilized for MIP synthesis, were optimized for the maximum development of DPASV current (Section S1 and Fig. S1).

2.7. Electrochemical procedure

Voltammetric measurements on bare and modified SPCEs were accomplished in a cell containing 10 mL phosphate buffer (optimized pH 7.5). The supporting electrolyte, phosphate buffer, was preferred to

other buffers (borate and acetate) because the later resulted in an asymmetric current, presumably due to the sluggish oxidation of HU. All DPASV runs were recorded, implicating the standard addition method, in the potential window 0.0 - + 0.6 V with the analyte accumulation (t_{acc}) 90 s and accumulated potential (E_{acc}) - 0.1 V at the scan rate 10 mV s^{-1}, pulse amplitude 25 mV, and pulse width 50 ms. CV runs were scanned in the same potential window as stated above, at various scan rates (20–200 mV s^{-1}), in anodic stripping mode. The de-aeration of the cell content was not required in this work because DPASV runs were found to be identical in the presence and absence of oxygen. (The operating analytical conditions were optimized as described in Section S2 and Fig. S2).

3. Results and discussion

3.1. Spectroscopic characterizations of N-GQDs and functionalized N-GQDs

The UV–Vis absorption spectrum of N-GQDs (Fig. 1A) shows two dominant absorption peaks at 231 nm and 335 nm, in addition to a broad absorption peak at 460 nm. These peaks could be associated to $\pi \rightarrow \pi^*$ transition of C=C bonds (Qu et al. 2013, 2014, 2015; Tang et al. 2012), $n \rightarrow \pi^*$ transition of C=O bonds (Qu et al. (2013)), and $n \rightarrow \pi^*$ transition of CN bonds (Qu et al., 2015), respectively. This suggests the N doping and presence of functional groups in N-GQDs. FT-IR spectrum was further used to identify the surface functional groups and chemical structure present in N-GQDs (Fig. 1B). The vibrational bands at 3464 (O-H stretch) and 1720 cm^{-1} (C=O stretch) corresponds N-GQDs having carboxylic acid. The absorption band at 1578 cm^{-1} correspond to the C=C stretching vibration of aromatic rings. The bands at 3349 (N-H asymmetrical), 3203 (N-H symmetrical), 1643 (amide-I), 1609 (amide-II), and 1215 cm^{-1} (C-N stretch.) reveal the successful introduction of N-containing groups and N-doping in the N-GQDs skeleton. These functional groups enhanced the hydrophilicity and stability of the N-GQDs in aqueous system, which supported the potentiality of the material for sensing in aqueous media.

Raman spectrum provided the convincing evidence for the microstructure of N-GQDs (Fig. 1C). N-GQDs showed D band (diamondoid mode) at 1320 cm^{-1} related to the presence of sp^3 defects, and G bands (graphite mode) at 1595 cm^{-1} corresponding to in-plane vibration of sp^2 carbon. Intensity ratio (I_D/I_G) of these bands could be used to compare the structural order between crystalline and amorphous graphitic system. The prepared N-GQDs exhibited I_D/I_G ratio 0.54, indicating the crystalline nature of N-GQDs. The functionalizations of N-GQDs were supported by FT-IR spectra (Fig. 1D). Accordingly, the appearance of C-Cl band at 593 cm^{-1} and disappearance of O-H band suggested the formation of acyl functionalized N-GQDs (N-GQDs-COCl) (Fig. 1D, curve a). Upon the reaction of N-GQDs-COCl with SDD, a new characteristic band was observed at 1073 cm^{-1} corresponding to C=S stretch, whereas the C-Cl band (593 cm^{-1}) was disappeared. This revealed the successful formation of iniferter N-GQDs (Fig. 1D, curve b). Formation of acrylated N-GQDs from N-GQDs-COCl was suggested by the disappearance of C=O (1745 cm^{-1}) and C-Cl stretch (593 cm^{-1}) bands (Fig. 1D, curve c) in the spectrum of acrylated N-GQDs.

3.2. Electrochemical characterization of modified electrodes

Electrochemical behaviors of fabricated SPCEs were carried out using $(Fe(CN)_6)^{3-/\ 4-}$ as probe. Fig. S3 showed a clear CV anodic-cathodic peak separation ($\Delta E_p = E_{pa} - E_{pc}$), on bare (curve a), AuNRs (curve b), Au/Ag NRs (curve c), Au/AgNRs@N-GQDs (curve d), Au/AgNRs-MIP (curve e), and Au/AgNRs@N-GQDs-MIP (curve f) modified SPCEs, to be 205, 185, 170, 110, 95, and 75, respectively. This revealed that the reversible behavior of electrode process was gradually increased from bare/SPCE to Au/AgNRs@N-GQDs-MIP/SPCE. This effect could be attributed to the presence of N-GQDs and Au/Ag NRs moieties in polymer skeleton, at the electrode selected for this study. Accordingly, the reversibility of electron-transfer reaction was found to be maximum with Au/AgNRs@N-GQDs-MIP/SPCE, on account of synergism in between N-GQDs and MIP, along with the inter-particle interactions between individual AuNR and Ag in bimetallic nanomaterials. It is noteworthy that individual pure metal (Au NRs) is found to be not as effective as bimetallic Au/Ag core-shell, in terms of reducing ΔE_p and increasing electrochemical surface area (A_{eff}) to enhance the current response (Table S1). Furthermore, CV responses of bare and modified SPCEs were found to be gradually increased. The maximum peak current was obtained for Au/AgNRs@N-GQDs-MIP/SPCE due to its larger A_{eff} as well as high roughness factor (R_f) 29.02, where $R_f = A_{eff}/A_{geom}$ and A_{geom} is the geometrical surface area (0.125 cm^2) of bare SPCE (Table S1). As a consequence, faster electrode kinetics was observed in comparison to other modified electrodes. For the calculation of A_{eff} of modified electrodes, the following Randles-Sevick equation was used (Bard and Faulker (2001)):

$$I_{pa} = (2.687 \times 10^5) n^{3/2} v^{1/2} D^{1/2} A_{eff} C^0 \quad (1)$$

where D (0.76×10^{-5} cm^2 s^{-1}) (Von Stackelberg et al., 1953) represents diffusion coefficient of ferricyanide; other parameters have their usual meanings. According to Table S1, A_{eff} and R_f values of Au/AgNRs@N-GQDs-MIP/SPCE were observed to be three-fold higher than Au/AgNRs-MIP/SPCE. This suggested that the intimate electronic interaction between N-GQDs and Au/AgNRs provided an exposed catalytic surface area, higher electrical conductivity, and high sensitivity for HU oxidation.

3.3. Spectral and morphological characterizations

Binding interactions between analyte and MIP were investigated on the basis of FT-IR (KBr) spectra of monomer (HPPD), analyte (HU), Au/AgNRs@N-GQDs-MIP-adduct, and Au/AgNRs@N-GQDs-MIP (Fig. S4). Accordingly, the analyte binding mechanism is proposed (Scheme 1), taking into account of downward shifts as a consequence of respective key bands participation in the complexation *via* hydrogen bond interactions (Section S3).

TEM was used to investigate the monodispersity and uniform size distribution of N-GQDs, AuNRs, and Au/Ag NRs (Fig. 2). Fig. 2A shows that N-GQDs are largely mono-dispersed (without agglomeration) with ~6 nm narrow size distribution in a low-contrast background. Fig. 2B clearly observes mono-dispersed AuNRs with aspect ratio of approximately 3.3. Furthermore, the nano core-shell superstructures of Au/Ag NRs (Fig. 2C) exhibited a corn-like shape due to the involvement of heterogeneous deposition of Ag atoms at the specific surface sites of the AuNRs. This effect could be feasible while avoiding the use of a reducing agent (such as ascorbic acid). EDS has been utilized to analyze the chemical compositions of AuNRs, Au/Ag NRs, and Au/AgNRs@N-GQDs nanohybrid (Section S4, Fig. S5).

SEM was used to analyze the morphology of the core-shell imprinted polymer modified SPCE surface. Fig. 3A and B show the polymer embodying texture. The morphology of Au/AgNRs@N-GQDs-MIP-adduct is quite compact. After template extraction, this turned to be porous to facilitate the fast diffusion of analyte molecules. Surface morphologies of Au/AgNRs@N-GQDs-MIP-adduct/SPCE (Fig. 3C) and Au/AgNRs@N-GQDs-MIP/SPCE (Fig. 3D) were also investigated with the help of AFM. Accordingly, the mean thickness of MIP film coating was found to be 113.2 nm (Section S5).

3.4. Electrochemistry of HU

CV runs showed a single anodic oxidation peak for HU performed on Au/AgNRs@N-GQDs-MIP/SPCE, at different scan rates (20–200 mVs^{-1}), in aqueous condition (Fig. 4A). However, the peak was shifted positively with increasing scan rates. This indicated some difficulty in analyte stripping, owing to more energy of oxidation required in the

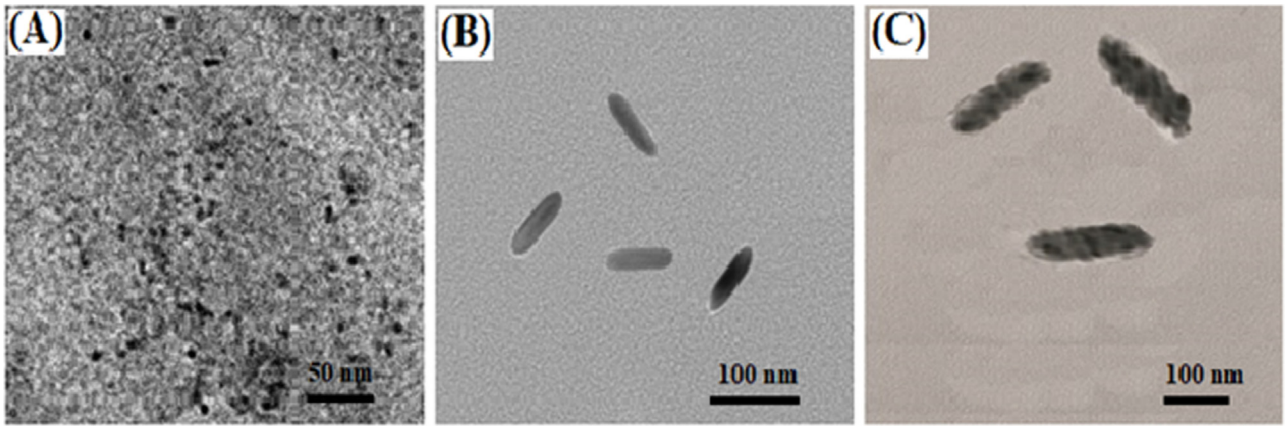

Fig. 2. TEM images: (A) N-GQDs, (B) Au NRs, and (C) Bimetallic Au/Ag core shell.

limited time span of higher scan rates. Anodic peak current (I_{pa}) increased with increase of scan rate (ν) in accordance to I_{pa} Vs $\nu^{1/2}$ (Eq. (2)) and anodic peak potential (E_{pa}) Vs log ν (Eq. (3)), which revealed the presence of a diffusion controlled phenomena:

$$I_{pa}(\mu A) = (2.648 \pm 0.540) + (17.722 \pm 1.675)v^{1/2}, \quad R^2 = 0.\ 97 \tag{2}$$

$$E_{pa}(V) = (0.502 \pm 0.007) + (0.107 \pm 0.006)\log v, \quad R^2 = 0.99 \tag{3}$$

Furthermore, a negative shift of oxidation peak was observed with the increase of pH of the medium (7.0–11.5). Notably, the analyte oxidation peak was not observed in acidic conditions; hence, the effect of pH was only seen in the basic range (7.0–11.5) in accordance to the following linear equation:

$$E_p(V) = (-0.053 \pm 0.009)pH + (0.628 \pm 0.082), R^2 = 0.97 \tag{4}$$

The slope of above linear equation revealed that protons and electrons were involved in equal ratio (1:1) for electro-oxidation of HU. The irreversibility of analyte oxidation at Au/AgNRs@N-GQDs-MIP/SPCE was based on the electron-transfer coefficient (α) value calculated using the following equation:

$$E_P = E^{0'} + \frac{RT}{(1-\alpha)nF}\ln v \tag{5}$$

where E_P is anodic peak potential, $E^{0'}$ the formal redox potential, n the number of electron transfer, v the scan rate, F the Faraday's constant, and R and T represent their usual meanings. The fractional value of α (0.49) supported the irreversible oxidation nature of HU.

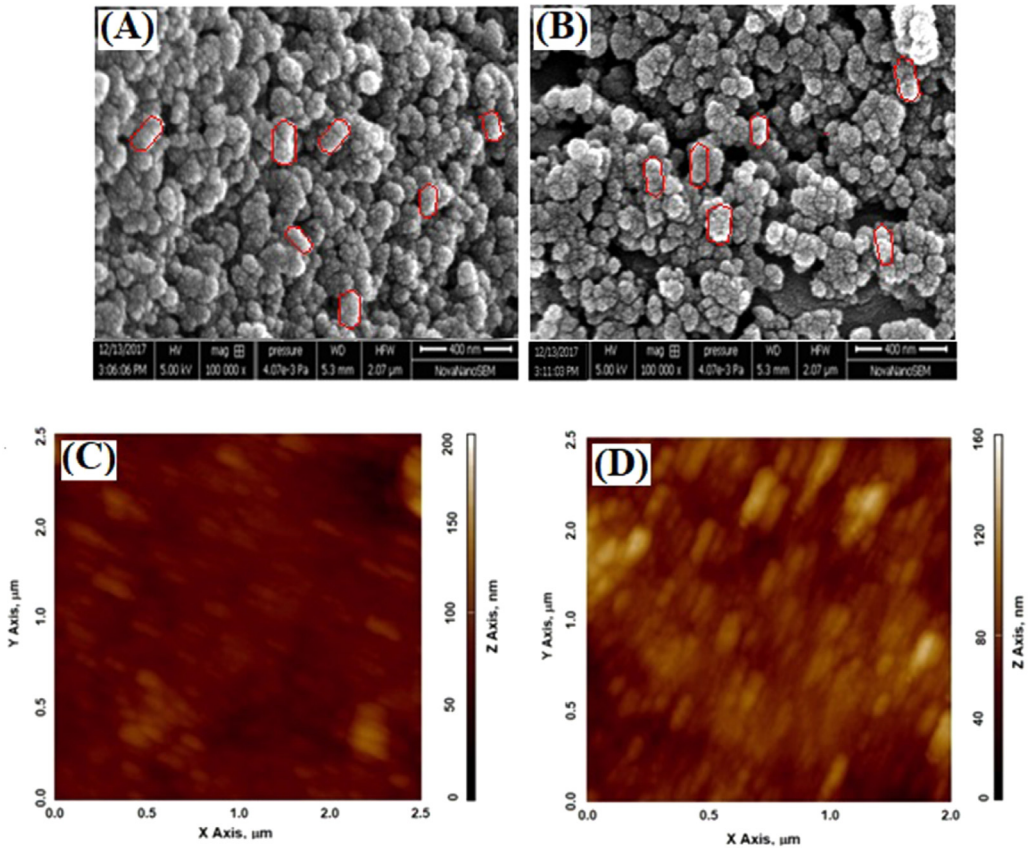

Fig. 3. (A) SEM image of Au/AgNRs@N-GQDs-MIP-adduct/SPCE, (B) SEM image of Au/AgNRs@N-GQDs-MIP/SPCE, (C) AFM image of Au/AgNRs@N-GQDs-MIP-adduct/SPCE, and (D)AFM image of Au/AgNRs@N-GQDs-MIP/SPCE.

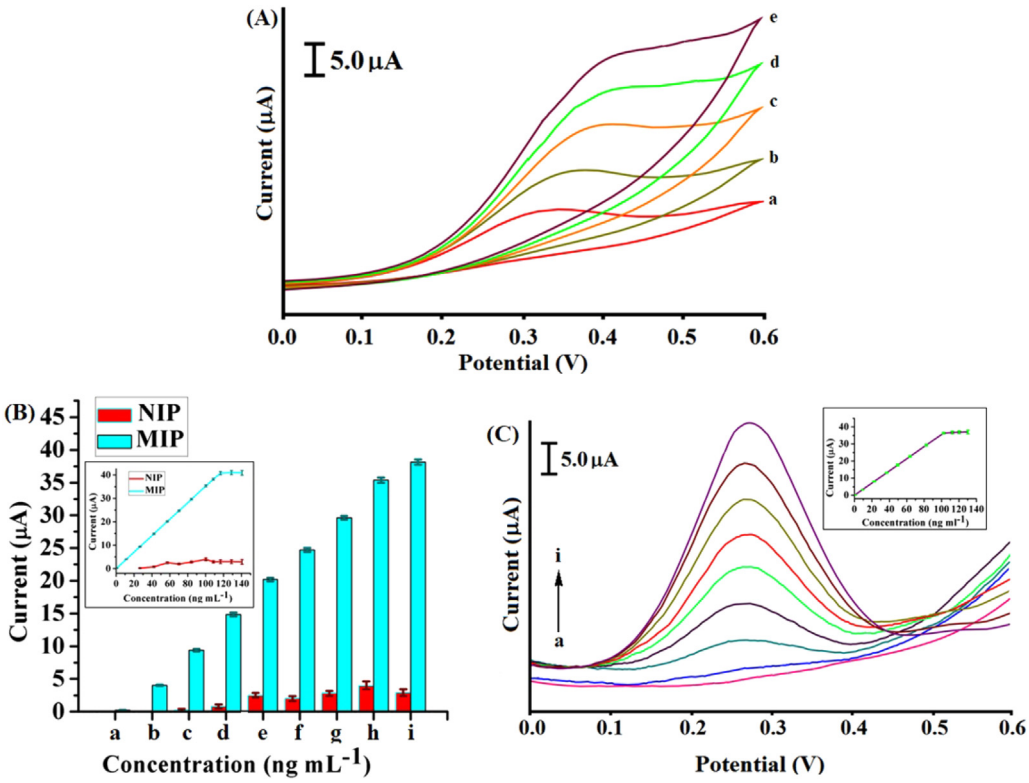

Fig. 4. (A) CV runs of HU (36.70 ng mL^{-1}) on Au/AgNRs@N-GQDs-MIP/SPCE at different scan rates: (a) 20, (b) 50, (c) 100, (d) 150, and (e) 200 mV s^{-1}. (B) DPASV responses on Au/AgNRs@N-GQDs-MIP and Au/AgNRs@N-GQDs-NIP modified SPCEs for different HU concentrations in aqueous environment (from a-i): 0.55, 11.29, 26.56, 42.12, 57.11, 70.14, 84.06, 101.11, and 108.44 ng mL^{-1} (Inset: Calibration plots at Au/AgNRs@N-GQDs-MIP-SPCE and Au/AgNRs@N-GQDs-NIP-SPCE in aqueous environment). (C) DPASV response on Au/AgNRs@N-GQDs-MIP/SPCE for HU in blood plasma (from a-i): 0.0, 0.62, 9.20, 22.56, 36.82, 49.60, 63.20, 82.40, and 102.33 ng mL^{-1} (Inset: Calibration plots at Au/AgNRs@N-GQDs-MIP-SPCE in blood plasma).

Estimation of standard heterogeneous rate constants (k) could be advantageous to comprehend the electrodics of Au/AgNRs@N-GQDs-MIP/SPCE. The k values were obtained to be 2.19×10^{-3} and 1.01×10^{-2} cm s^{-1} at Au/AgNRs-MIP/SPCE and Au/AgNRs@N-GQDs-MIP/SPCE, respectively. The higher k value for analyte oxidation at Au/AgNRs@N-GQDs-MIP/SPCE indicated fast electrode kinetics, owing to the effective electron mediation of Au/AgNRs@N-GQDs nanohybrid toward the analyte oxidation. Accordingly, the covalently bound Au/AgNRs@N-GQDs nanohybrid with MIP (monomer) trapped electrons in its quantum confinement and donated them easily to the electrode surface, without any interfacial barrier. On the other hand, Au/Ag NRs-MIP interface (randomly dispersed Au/Ag NRs residues in MIP-film) might not have relatively effective electronic mediation at SPCE surface.

Chronocoulometric measurements were performed on both types of MIP modified SPCEs in the phosphate buffer (pH 7.5). Accordingly, the surface coverage (Γ^{0}) with 6.63×10^{11} molecules and 1.61×10^{13} molecules and diffusion coefficient (D) values 4.30×10^{-6} and 9.08×10^{-5} cm^2 s^{-1}, were obtained on Au/AgNRs-MIP/SPCE and Au/AgNRs@N-GQDs-MIP/SPCE, respectively. Both Γ^{0} and D on Au/AgNRs@N-GQDs-MIP/SPCE were found to be approximately 20 times higher than Au/AgNRs-MIP/SPCE. These values revealed that the molecular texture of Au/AgNRs@N-GQDs-MIP nanocomposite was adequately organized to render homogeneous binding sites (effective surface area) and to channelize the pathway for faster ingress and egress of the analyte (Section S6).

To evaluate the spontaneity of analyte adsorption from bulk to the respective homogeneous MIP cavities, Langmuir adsorption isotherm is adjudged better in this work. Homogeneous MIP cavities possess well defined binding sites, in which each site holds one molecule, without any mutual interaction with other immobilized molecules. On the other hand, the Freundlich isotherm is applicable only for the multilayer adsorption on the heterogeneous surface of sorbent and is non-accountable to define the maximum adsorption beyond a saturation point. Thus, in the present instance, all chronocoulometric data of analyte adsorption in the MIP monolayer could be best fitted in the Langmuir adsorption isotherm. The adsorption coefficient (b) and Gibbs free energy (ΔG) were found to be 4.13×10^{8} L mol^{-1} and - 49.16 kJ mol^{-1}, respectively. The higher b value reflected a strong binding affinity of the analyte molecules within MIP cavities and negative value of ΔG suggested spontaneity for the adsorption of analyte (Section S7).

Electrical conductivities of MIP nanocomposites were measured using the two-probe technique. The Au/AgNRs@N-GQDs-MIP showed approximately 30-folds higher electrical conductivity than the Au/AgNRs-MIP (Au/AgNRs@N-GQDs-MIP: 7.4×10^{-3} S cm^{-1}, Au/AgNRs-MIP: 2.3×10^{-3} S cm^{-1}). BET surface areas of MIP nanocomposites were also obtained to be 157.71 and 113.27 m^2 g^{-1} for Au/AgNRs@N-GQDs-MIP and Au/AgNRs-MIP, respectively (Section S8).

3.5. Analytical performance

Analytical performances of Au/AgNRs@N-GQDs-MIP/SPCE and Au/AgNRs@N-GQDs-NIP/SPCE for the detection of HU were studied in aqueous and real samples (human blood plasma, human urine and pharmaceuticals), under optimized operating conditions of DPASV measurements. The excellent linearity between I_p and C was noticed with, quantitative HU recoveries and limits of detections (*LODs*) (0.04–0.07 ng mL^{-1}) (Table 1, Fig. 4B). The *LODs* were calculated as three times of the standard deviation obtained in blank divided by the slope of the calibration plot between HU concentration and DPASV current (Skoog et al., 1998). However, the NIP modified SPCE did not respond any linearity (R^2 = 0.81) with concentrations (Fig. 4B, inset). Fortuitously, such nonspecific adsorption of analyte at NIP modified SPCE could be washed away with water (1.5 mL, n = 3). Thus, the MIP modified SPCE was also given the similar washing treatment, as safeguard. Interestingly, DPASV currents for HU at MIP modified SPCE in blood plasma were highly symmetrical, like that obtained in aqueous media (Fig. 4C). This reflected similar sample behavior of diluted real samples, akin to aqueous media. The proposed sensor has been compared with earlier known methods/electrodes for HU determination (Table S2). Accordingly, most of the earlier methods/electrodes had poor sensitivity and selectivity and no study with interferences were

Table 1
Sample behavior.

Sample	Regression equation	Range (ng mL^{-1})	Recovery[a] (%)	LOD^{b} (3σ) (ng mL^{-1})	RSD^{c} (%) (n = 3)
Aqueous	I_p = (0.3520 ± 0.0004)C + (0.0336 ± 0.027), n = 9, R^2 = 0.99	0.55–108.43	98.2 – 101.7	0.05	0.12
Blood plasma (diluted 100 times)	I_p = (0.3558 ± 0.0003)C + (0.0224 ± 0.021), n = 8, R^2 = 0.99	0.62–102.33	98.2 – 101.4	0.07	0.10
Pharmaceutical[d] (diluted 8.7×10^7 times)	I_p = (0.3472 ± 0.0002)C + (0.0303 ± 0.017), n = 7, R^2 = 0.99	0.57–107.33	99.1–100.5	0.04	0.48
Urine (diluted 100 times)	I_p= (0.3535 ± 0.0002)C + (0.0130 ± 0.011), n = 7, R^2 = 0.99	0.65–101.56	99.2 – 100.7	0.06	0.05

[a] % Recovery = (amount of analyte determined / amount of analyte taken) × 100.
[b] *LOD* based on the minimum distinguishable signal for lower concentrations of analyte (S/N = 3, 95% confidence level).
[c] *RSD* (%) for three sets of *LOD* data.
[d] Endogenous HU (concentration of drug obtained × dilution factor) is obtained as 5.0×10^7 ng mL^{-1} which is in agreement with the certified value.

made. On the contrary, the proposed sensor showed high sensitivity and selectivity for HU in real samples, without any sample pre-treatment, despite the critical limitation of MIP procurement for this purpose.

3.6. Interference and endurance studies

To evaluate cross-selectivity of the proposed sensor, DPASV responses of HU in the presence of some interfering compounds viz; anticancer drugs (temozolomide (TMZ) dacarbazine (Dac), ifosfamide (Ifos) and chlorambucil (Chloram)), biomolecules (urea, uric acid (UA), citric acid (CA), cystien (Cys), phenyl alanine (Phe), ascorbic acid (AA), and DA), and their mixtures were recorded at MIP and NIP-modified SPCEs (Fig. S6). MIP and NIP modified SPCEs showed a feeble DPASV response for all individual interferent compounds, without undergoing any water-washing. The binary mixture of HU and interferent(s), particularly taken in 1:1 and 1:100 concentration ratios, were also examined. In the binary mixtures, the MIP-modified sensor yielded a quantitative (100%) response of HU. To further confirm the selectivity of the proposed sensor, selectivity coefficients (k), relative selective coefficients (k'), and imprinting factor ($I.F. = I_{MIP}/I_{NIP}$) were calculated and portrayed in Table S3. This suggested that the proposed sensor was capable for quantitative analysis of HU in real samples, even in the presence of the higher concentration of interferent(s). Thus, a phenomenal imprinting effect ($I.F.$ = 18.6) was observed. The reproducibility, regeneration and stability of proposed sensor were discussed in the supporting information as Section S.9 and Fig. S7. Accordingly, the proposed sensor was stable with good endurance and reproducibility for practical uses within 20 days. The regeneration of electrode was feasible by method of template retrieval using methanol as solvent for 20 binding-rebinding cycles.

4. Conclusions

For the first time, Au/AgNRs@N-GQDs-MIP modified SPCE sensor was developed for ultra-trace sensing of HU in aqueous/real samples. This includes a nanohybrid of functionalized N-GQDs and bimetallic Au/Ag core shell to serve as an effective electron mediator. Further it was found to be advantageous in terms of heterogeneous rate constant (1.01×10^{-2} cm s^{-1}), diffusion coefficient (9.08×10^{-5} cm^2 s^{-1}), conducting capacity (7.4×10^{-3} S cm^{-1}), and securing stable coating including efficient electro-catalytic action as compared with Au/AgNRs-MIP. The proposed sensor was highly specific and sensitive (*LODs,* 0.05 (aqueous), 0.07 (blood plasma), 0.04 (pharmaceutical), and 0.06 ng mL^{-1} (urine)), with phenomenal imprinting ($I.F.$ = 18.6) in the aqueous environment. Similar results were realized with real samples. Although the sensor fabricated requires somewhat a lengthy protocol for MIP synthesis, it could be undoubtedly used for deciding oral supplementation of anticancerous HU in clinical patients.

Acknowledgement

Authors acknowledge technical assistance received from the Institute of Science, Banaras Hindu University, Varanasi, India.

Appendix A. Supplementary material

Supplementary data associated with this article can be found in the online version at doi:10.1016/j.bios.2018.11.055.

References

Amjadi, M., Jalili, R., 2016. RSC Adv. 6, 86736–86743.
Aoun, S.B., 2017. R. Soc. Open Sci. 4, 171199.
Bachir, D., Hulin, A., Huet, E., Habibi, A., Nzouakou, R., El Mahrab, M., Astier, A., Galacteros, F., 2007. Hemoglobin 31, 417–425.
Bard, A.J., Faulker, L.R., 2001. Electrochemical Methods, 2nd ed. Wiley, New York.
Cai, F., Liu, X., Liu, S., Liu, H., Huang, Y., 2014. RSC Adv. 4, 52016–52022.

Chen, Y.-X., Huang, K.-J., Niu, K.-X., 2018a. Biosens. Bioelectron. 99, 612–624.
Chen, Y.-X., Huang, K.-J., He, L.-L., Wang, Y.-H., 2018b. Biosens. Bioelectron. 100, 274–281.
Chizari, K., Janowska, I., Houllé, M., Florea, I., Ersen, O., Romero, T., Bernhardt, P., Ledoux, M.J., Pham-Huu, C., 2010. Appl. Catal. A: Gen. 380, 72–80.
Choi, H.-J., Jung, S.-M., Seo, J.-M., Chang, D.W., Dai, L., Baek, J.-B., 2012. Nano Energy 1, 534–551.
Dai, L., Song, L., Huang, Y., Zhang, L., Lu, X., Zhang, J., Chen, T., 2017. Langmuir 33, 5378–5384.
Das, A., Sangaranarayanan, M.V., 2015. Electroanalysis 27, 360–367.
Dong, Y., Shao, J., Chen, C., Li, H., Wang, R., Chi, Y., Lin, X., Chen, G., 2012. Carbon 50, 4738–4743.
Elias, D.B.D., Carvalho, T.M.J.P., Soares, J.E.S., Gonçalves, R.P., 2014. Braz. J. Pharm. Sci. 50, 621–628.
Endo, T., Kerman, K., Nagatani, N., Hiepa, H.M., Kim, D.-K., Yonezawa, Y., Nakano, K., Tamiya, E., 2006. Anal. Chem. 78, 6465–6475.
Geng, D., Ding, N., Andy Hor, T.S., Liu, Z., Sun, X., Zong, Y.J., 2015. Mater. Chem. A 3, 1795–1810.
Gordon, A., Asante, S.B., Bukari, Y., Gati, L., Osei-Adjei, G., Hackman, H.K., Asare, E.O., 2015. RA J. Appl. Res. 1, 235–242.
Gowda, S.K.N., Mahendra, K.N., 2006. Bull. Korean Chem. Soc. 27, 1542–1548.
Hai, X., Guoa, M., Gaoa, C., Zhoub, J., 2017. J. Pharm. Biomed. Anal. 137, 213–219.
Hsu, S.-W., On, K., Gao, B., Tao, A.R., 2011. Langmuir 27, 8494–8499.
Huang, Y., Ferhan, A.R., Kim, D.H., 2013a. Nanoscale 5, 7772–7775.
Huang, Y., Wu, L., Chen, X., Bai, P., Kim, D.-H., 2013b. Chem. Mater. 25, 2470–2475.
James, H., Nahavandi, M., Wyche, M.Q., Taylor, R.E., 2006. J. Chromatogr. B 831, 42–47.
Jiang, D., Zhang, Y., Chu, H., Liu, J., Wan, J., Chen, M., 2014. RSC Adv. 4, 16163–16171.
Jiang, H.-L., Akita, T., Ishida, T., Haruta, M., Xu, Q., 2011. J. Am. Chem. Soc. 133, 1304–1306.
Jong, H.Y.J., Hsub, O., Wu, H.L., Kou, H.S., Wu, S.M., 2003. Anal. Chim. Acta 488, 223–230.
Ju, J., Chen, W., 2014. Biosens. Bioelectron. 58, 219–225.
Kailasa, S.K., Wu, H.F., 2012. Analyst 137, 1629–1638.
Kashani, H.M., Madrakian, T., Afkhami, A., 2017. New J. Chem. 41, 6875–6882.
Kettani, T., Cottona, F., Gulbis, B., Ferster, A., Kumps, A., 2009. J. Chromatogr. B 877, 446–450.
Kumawat, M.K., Thakur, M., Gurung, R.B., Srivastava, R., 2017. Sci. Rep. 7, 15858.
Li, L., Li, L., Wang, C., Liu, K., Zhu, R., Qiang, H., Lin, Y., 2015. Microchim. Acta 182, 763–770.
Li, Q., Zhang, S., Dai, L., Li, L., 2012b. J. Am. Chem. Soc. 134, 18932–18935.
Li, Y., Zhao, Y., Cheng, H., Hu, Y., Shi, G., Dai, L., Qu, L., 2012a. J. Am. Chem. Soc. 134, 15–18.
Lin, L., Rong, M., Lu, S., Song, X., Zhong, Y., Yan, J., Wang, Y., Chen, Xi, 2015. Nanoscale 7, 1872–1878.
Liu, G., Wu, Z., Wang, S., Shen, G., Yu, R., 2001. Anal. Chem. 73, 3219–3226.
Ma, Y., Li, W., Cho, E.C., Li, Z., Yu, T., Zeng, J., Xie, Z., Xia, Y., 2010. ACS Nano 4, 6725–6734.
Maier, S.A., Atwater, H.A., 2005. J. Appl. Phys. 98, 011101–011110.
Majid, Z.W., Bashir, W.A., 2013. Rafidain J. Sci. 24, 53–64.
Marahatta, A., Megaraj, V., McGann, P.T., Ware, R.E., Setchell, K.D.R., 2016. Clin. Chem. 62, 1593–1601.
Naik, K.M., Nandibewoor, S.T., 2014. J. Electrochem. Sci. Eng. 4, 111–121.
Naik, K.M., Alagur, M.M., Nandibewoor, S.T., 2013. Anal. Methods 5, 6947–6953.
Naik, K.M., Ashi, C.R., Nandibewoor, S.T., 2015. J. Electroanal. Chem. 755, 109–114.
Prasad, B.B., Rai, G., 2013. Spectrochim. Acta A Mol. Biomol. Spectrosc. 105, 400–411.
Prasad, B.B., Kumar, A., Singh, R., 2017. Biosens. Bioelectron. 94, 1–9.
Qu, D., Zheng, M., Du, P., Zhou, Y., Zhang, L., Li, D., Tan, H., Zhao, Z., Xie, Z., Sun, Z., 2013. Nanoscale 5, 12272–12277.
Qu, D., Zheng, M., Zhang, L., Zhao, H., Xie, Z., Jing, X., Haddad, R.E., Fan, H., Sun, Z., 2014. Sci. Rep. 4, 5294.
Qu, D., Sun, Z., Zheng, M., Li, J., Zhang, Y., Zhang, G., Zhao, H., Liu, X., Xie, Z., 2015. Adv. Opt. Mater. 3, 360–367.
Razmi, H., Mohammad-Rezaei, R., 2013. Biosens. Bioelectron. 41, 498–504.
Rodriguez, A., Beukens, D., Debouge, N., Gulbis, B., Cotton, F., 2014. J. Chromatogr. 5, 1–4.
Roushani, M., Abdi, Z., 2014. Sens. Actuators B-Chem. 201, 503–510.
Samal, A.K., Polavarapu, L., Rodal-Cedeira, S., Liz-Marzán, L.M., Pérez-Juste, J., Pastoriza- Santos, I., 2013. Langmuir 29, 15076–15082.
Shi, B., Zhang, L., Lan, C., Zhao, J., Su, Y., Zhao, S., 2015. Talanta 142, 131–139.
Skoog, D.A., Holler, F.T., Neiman, T.A., 1998. Principles of Instrumental Analysis, 5th ed. Harcourt Brace College Publishers, Orlando.
Sun, G., Liu, H., Zhang, Y., Yu, J., Yan, M., Song, X., 2015. New J. Chem. 39, 6062–6067.
Tam, T.V., Trung, N.B., Kim, H.R., Jin, Chung, S., Choi, W.M., 2014. Sens. Actuators B 202, 568–573.
Tan, F., Cong, L., Li, X., Zhao, Q., Zhao, H., Quan, X., Chen, J., 2016. Sens. Actuators B Chem. 233, 599–606.
Tang, L., Ji, R., Cao, X., Lin, J., Jiang, H., Li, X., Teng, K.S., Luk, C.M., Zeng, S., Hao, J., Lau, S.P., 2012. ACS Nano 6, 5102–5110.
Usawanuwat, J., Boontanon, N., Boontanon, S.K., 2014. Int. J. Adv. Agric. Environ. Eng. 1, 72–76.
Vasilescu, A., Andreescu, S., Bala, C., Litescu, S.C., Noguer, T., Marty, J.L., 2003. Biosens. Bioelectron. 18, 781–790.
Von Stackelberg, M.V., Pilgram, M.Z., Me, V.I., 1953. Elektrochemie 57, 342–350.
Wang, D.-W., Su, D., 2014. Energy Environ. Sci. 7, 576–591.
Wang, Y., Shao, Y., Matson, D.W., Li, J., Lin, Y., 2010. ACS Nano 4, 1790–1798.
Wang, Y.-H., Huang, K.-J., Wu, X., 2017. Biosens. Bioelectron. 97, 305–316.
Yang, Y., Liu, Q., Liu, Y., Cui, J., Liu, H., Wang, P., Li, Y., Chen, L., Zhao, Z., Dong, Y., 2017. Biosens. Bioelectron. 90, 31–38.
Ye, X., Zheng, C., Chen, J., Gao, Y., Murray, C.B., 2013. Nano Lett. 13, 765–771.
Zhang, S., Wright, G., Yang, Y., 2000. Biosens. Bioelectron. 15, 273–282.
Zhao, J., Chen, G.F., Zhu, L., Li, G.X., 2011. Electrochem. Commun. 13, 31–33.
Zhou, X., Wang, A., Yu, C., Wu, S., Shen, J., 2015. ACS Appl. Mater. Interfaces 7, 11741–11747.
Zor, E., Morales-Narváez, E., Zamora-Gálvez, A., Bingol, H., Ersoz, M., Merkoçi, A., 2015. ACS Appl. Mater. Interfaces 7, 20272–20279.